JOURNAL OF CHEMICAL INFORMATION AND MODELING

ARTICLE

pubs.acs.org/jcim

Conformational Enantiomerization and Estrogen Receptor α Binding of Anti-Cancer Drug Tamoxifen and Its Derivatives

Li Gao,[†] Yaoquan Tu,[†] Pia Wegman,[‡] Sten Wingren,[‡] and Leif A. Eriksson[*,†,§]

[†]Örebro Life Science Center, School of Science and Technology, Örebro University, 70182 Örebro, Sweden

[‡]Department of Health and Medical Sciences, Örebro University, 70182 Örebro, Sweden

[§]School of Chemistry, National University of Ireland, Galway, Ireland

Supporting Information

ABSTRACT:

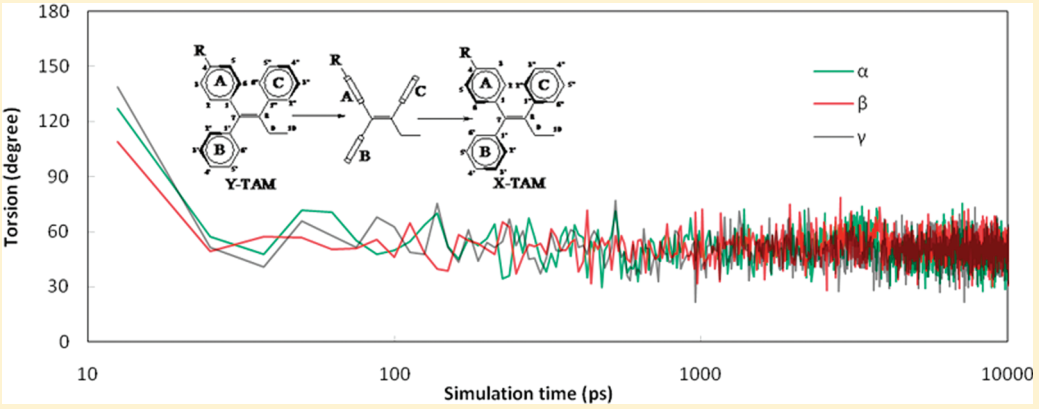

The anticancer drug tamoxifen (TAM) displays two chiral vinyl propeller structures, which interconvert so rapidly that the process is undetectable on the NMR time scale. In the present work, the enantiomerization processes were investigated with molecular modeling techniques. The threshold mechanisms probed at the different rings were shown to be identical, i.e., involving a synchronous three-ring flip, with a correlated rotation of the rings. In order to reveal the pharmacological profiles of the two chiral forms, we performed structural studies on the ligand binding domain of estrogen receptor α (ERα LBD) and associated ligands. The enantiomers, with opposite torsional twist, were found to be discriminated by ERα. For TAM and its main metabolites, the effects of the stereoselectivity of ERα are overcome by the low energy cost for helical inversion between the two torsional enantiomers, estimated to be ~3 kcal/mol.

1. INTRODUCTION

Breast cancer is the most common cancer among women, with increasing prevalence. Because of early diagnosis and better treatments, the disease-specific death rate has declined considerably in recent years. Tamoxifen (TAM) is the most important therapeutic selective estrogen receptor modulator (SERM) for the treatment of hormone receptor expressing breast cancer. It has been used for more than 30 years as a first-line drug in endocrine therapy of breast cancer,[1,2] providing a significant reduction in the risk of recurrence.[3] TAM and its metabolites competitively bind to estrogen receptor α (ERα) and inhibit the binding of estradiol, and therefore, function as estrogen antagonists in breast cancer tissues and block the proliferation of breast cancer cells otherwise triggered by estradiol.[4] TAM, the parent drug, is a weak anti-estrogen with fairly weak affinity to its target ERα. It is extensively metabolized by the cytochrome P450 enzymes, whereby it is mainly converted to the N-desmethyl and 4-hydroxyl metabolites.[5,6] The 4-hydroxyl metabolites of tamoxifen, 4-hydroxytamoxifen (OHT), and 4-OH-N-desmethyl-TAM (edoxifen), are the most important metabolites as potent anti-estrogens with much higher affinity to ER compared to tamoxifen.[7,8]

Chemically, TAM is a triphenylethylene derivative. X-ray structures have confirmed that crystalline TAM has a propeller type structure,[9] as do other triarylvinyl class of compounds.[10] The aryl groups (the "propeller blades", attached to an ethylenic double bond) are twisted in the same sense, although with different values of the torsional angles.[11] An intriguing property of torsion, especially for TAM analogues, is the intrinsic chirality

Received: October 13, 2010
Published: December 31, 2010

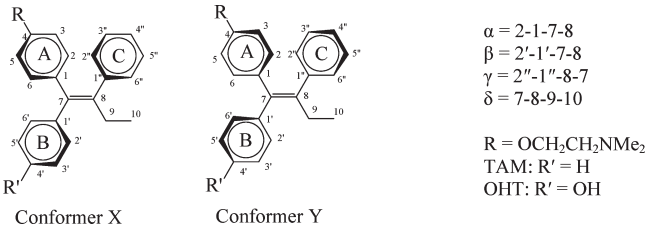

Figure 1. Enantiomers and definition of torsional angles in TAM and OHT.

in that the torsional isomers differ in helicity. When all the rings have local C_2 axis, the systems exists in enantiomeric pairs, in which all three rings are twisted in the opposite sense. The enantiomers (atropisomers) display a "clockwise" propeller with conformer X, and conversely, conformer Y has a "counterclockwise" propeller (Figure 1).

The propeller conformations are energetically favored over other structures, due to reduced steric repulsion, and at the same time maximized conjugation of the aryl rings. The twisting of the rings in a correlated rotation results from a compromise between the conjugation and steric effects, yielding the atropisomers as low-energy conformers.[12,13] The interconversion between the isomers has been extensively studied for the vinyl propellers of triarylvinyl systems.[10,12,14−18] Dynamic NMR (DNMR) detection is often used in the experimental study of the competing isomerization routes and to determine the corresponding rotational barriers. The lowest activation energy mechanism (threshold mechanism) determines the rate of the interconversion. The three-ring flip has been found to be the threshold rotational mechanisms for most crowded vinyl propellers, with energy barriers of 15−20 kcal/mol.[10,12,15,17] However, experimental data is limited for the less crowded TAM propeller, as the enantiomerization process is rapid and not detectable on the NMR time scale, neither at room temperature nor at −75 °C.[19] The interconversion between the enantiomers could be even faster at physiological temperature. Using molecular mechanics (force field based) computations, the interconversion between the isomers of TAM was observed to occur in the time range of picoseconds.[13] Therefore, the anticancer drug TAM is transformed rapidly by thermal equilibration to racemates in the physiological environment. The pharmacological profiles of the two chiral forms are thus not possible to detect experimentally and are still poorly understood. In addition, the data on the barriers for the different alternative enantiomerization routes are limited for TAM and the in vivo metabolites. In the current work, quantum chemical calculations were performed to study the competing enantiomerization routes of TAM and its metabolites. These results, in conjunction with structural modeling and molecular dynamics simulations of ERα, were used to analyze the binding action of the anticancer drug TAM and its key metabolites. Of particular focus is the distinction of the pharmacological profiles of the two chiral forms.

2. METHODOLOGY

Quantum Chemical Calculations. Calculations of the threshold mechanisms were carried out using density functional theory (DFT). The hybrid exchange-correlation functional B3LYP[20−22] with the 6-31+G(d,p) basis set was mainly used for the geometry optimizations and studies on the rotational enantiomerization routes in vacuo. B3LYP and the pure exchange-correlation functional BLYP with the 6-311++G-(2d,2p) basis set were used for better estimates of the rotational barriers. Frequency calculations were performed on the optimized geometries to ensure the structures to be transition states or local minima and to extract free energy corrections. To mimic the molecules under physiological conditions, we used the protonated forms of the TAM derivatives. General solvent effects were considered using the SMD continuum solvation model,[23] based on the quantum mechanical charge density of the solute molecules. Single-point calculations in aqueous solution (ε = 78.36) were carried out on the optimized geometries at the same level of theory. All calculations were performed using the Gaussian09 program package.[24]

Table 1. Torsional Angles of the Low-Energy Structures of TAM Optimized at the B3LYP/6-31+G(d,p) Level, Compared with X-ray Data

	torsional angle (degrees)				
conformer	α	β	γ	δ	energy (a.u.)
Y	−48	−62	−58	115	−1138.63293
X	47	63	59	−114	−1138.63276
X-ray data (Y)	−48	−64	−55	114	

As an initial set of test calculations, DFT-based geometry optimizations were performed for TAM using a range of different exchange-correlation functionals. All the functionals tested gave torsional angles of the Y conformer comparable to X-ray data, with the B3LYP and BLYP optimized geometries in best agreement with experiments (Table S1 of the Supporting Information). For another similar highly conjugated biphenyl system calculated by Johansson et al., B3LYP was found to perform as well as other high level ab initio methods.[25] We are thus confident that the current approach provides data of sufficiently high accuracy.

Molecular Mechanics Modeling. Molecular modeling of the ERα complexes was performed with the Molecular Operating Environment (MOE) program, version 2009.10.[26] Crystallographic structures of the ligand binding domain (LBD) of ERα-SERM complexes were obtained from the RCSB Protein Data Bank (PDB). OHT-ERα LBD (PDB no. 3ERT/2JF9/2BJ4), GW5638-ERα LBD (PDB no. 1R5K) Raloxifene-ERα LBD (PDB no. 1ERR), lasofoxifene-ERα LBD (PDB no. 2OUZ), and benzoxathiin derivative-ERα LBD (PDB no. 01SJ) were used in structural alignments and the calculations of root-mean-square deviation (rmsd) of C-α atoms.

In order to predict the atomic motions of X/Y-TAM in the ERα binding site, molecular dynamics (MD) simulations were conducted with YASARA v10.7.20,[27] using the AMBER03[28] force field. The partial atomic charges of the ligands were computed using the AM1-BCC model[29] implemented in YASARA. The net charge was +1 for both OHT and TAM, with the nitrogen atom protonated. The crystal structure of OHT-ERα LBD (PDB no. 3ERT) was used as the starting point. X/Y-TAM was introduced by removing the hydroxyl group of OHT in 3ERT and resetting the dihedrals. MD simulations in explicit water were performed at a constant temperature (298 K) after initial energy minimization procedures. Periodic boundary conditions were applied to the system, and counterions were added by randomly replacing water molecules by Na^+ or Cl^- to provide a charge-neutral system and to give a total NaCl concentration

dx.doi.org/10.1021/ci100401t |J. Chem. Inf. Model. 2011, 51, 306–314

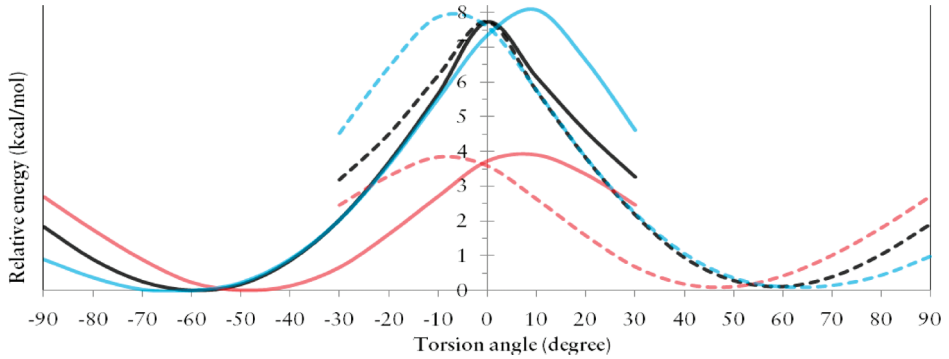

Figure 2. Potential energies as functions of the torsional angles for internal rotations around the C(Ar)−C(sp^2) bonds for TAM. The calculations were carried out at the B3LYP/6-31+G(d,p) level, with both Conformer X (dashed lines) and Conformer Y (solid lines) as starting geometries. The correlated rotations are calculated with the rotation initiated from each single ring: A-ring (α, red), B-ring (β, blue), and C-ring (γ, black).

of 0.9% corresponding to physiological solution. Long-range Coulomb interactions were included using particle-mesh Ewald (PME) summation and a cutoff of 7.86 Å. The simulations were carried out in their entirety, using a predefined macro (md_run) within the YASARA package. Multiple time steps used in the simulation were 1.25 fs for intramolecular and 2.5 fs for intermolecular forces, and data were collected every 12.5 ps. Three independent 10 ns simulations were conducted for each system as outlined below.

3. RESULTS AND DISCUSSION

3.1. Quantum Chemical Studies on Threshold Enantiomerization Mechanisms of TAM Derivatives. The vinyl propellers are intrinsically chiral, and the enantiomers have reverse helicity through an opposite torsional twist of the propeller blades. The torsional angles of the TAM/OHT propellers are shown in Figure 1. Conformer X, with a "clockwise" propeller, corresponds to positive values of the torsional angles α, β, and γ. Conversely, conformer Y, with a "counterclockwise" propeller, corresponds to negative values of α, β, and γ.

Interchange between the enantiomers due to torsional rotation of the vinyl propellers was investigated by quantum chemical calculations. Diastereomerization due to the overall C_1 symmetry was not considered. A difference in helicity (i.e., propeller blades in opposite directions) is the only structural feature differing in the torsional enantiomers. The hybrid DFT functional B3LYP was used for the geometry optimization of TAM; the results are shown in Table 1. The helical enantiomers were identified as low-energy conformers, with a negligible energy difference between the two mirror images. The B3LYP functional in conjunction with the 6-31+G(d,p) basis set give torsional angles (conformer Y) very close to the X-ray data. Similar computational results were reported in previous studies;[13,30] although the torsional angles obtained in this work are slightly closer to those found in the crystalline sample.

NMR studies have indicated that the enantiomerization of TAM in solution is too rapid to be detectable on the NMR time scale.[19] We studied the rotational processes of the TAM vinyl propellers by calculating the internal rotations around the C(Ar)−C(sp^2) bonds, connecting the aryl rings to the ethenyl group. Competing enantiomerization routes were investigated, starting from a single ring rotation, with correlated rotations of the other two rings. The results are shown in Figure 2. The two low-energy conformers X and Y were chosen as starting geometries for the calculations, represented as the minima of each potential energy curve. Conformer X corresponds to the torsional angle values 47°, 63° and 59° for α, β, and γ, respectively, while conformer Y corresponds to −48°, −62°, and −58°, respectively. The relative energies represent the activation energies for correlated rotation of the three rings, although in each case initiated by rotating one single ring. For the vinyl propeller, the four carbon atoms connecting to the double bond are not strictly coplanar. This results in slight unsymmetrical rotations around the C(Ar)−C(sp^2) bonds as reflected in the potential energy curves, where the torsional angles corresponding to the maxima are shifted away slightly from 0°.

Helicity reversal in TAM propellers proceeds by correlated rotation of the three "blades". The potential energy curves in Figure 2 show different ways for the helicity reversal from conformer X to Y or vice versa. For the correlated rotation, the initiating ring rotates either through the double-bond plane (∼0°) or the perpendicular plane (∼90°), referred to as "nonflip" (∼0°) or "flip" (∼90°), respectively. Conformer X was chosen as the starting geometry to search for the rotational transition states of distinct enantiomerization processes, and the competing rotational routes were investigated starting from the rotation of each single ring. No matter if the rotation-initiating ring passes through the double-bond plane (noflip) or the perpendicular plane (flip), the other two rings flip concurrently through the perpendicular planes resulting in the helical reversion of the vinyl propeller. The competing enantiomerization mechanisms are depicted in Figure 3 by idealized structures of the vinyl propeller.

For each single ring rotation through the double-bond plane (nonflip), there are distinct transition states as shown in Figure 3, corresponding to the rotations initiated from the A-, B-, or C-ring. The torsional angles of the noflip rings deviate slightly from 0° at the optimized transition states, as seen in Figure 2 and Table 2. The other two rings flip simultaneously through the perpendicular planes, therefore designated as two-ring flip mechanisms.

There is only one transition state for the motion involving all three rings to go through the perpendicular plane (flip), regardless of whether the rotation starts from the A-, B-, or C-ring. As all three rings pass through the perpendicular planes concurrently, this pathway was referred to as the three-ring flip (Figure 3). The torsional angles at the transition state are 92°, 110°, and 76° for α, β, and γ, respectively, differing slightly from 90°.

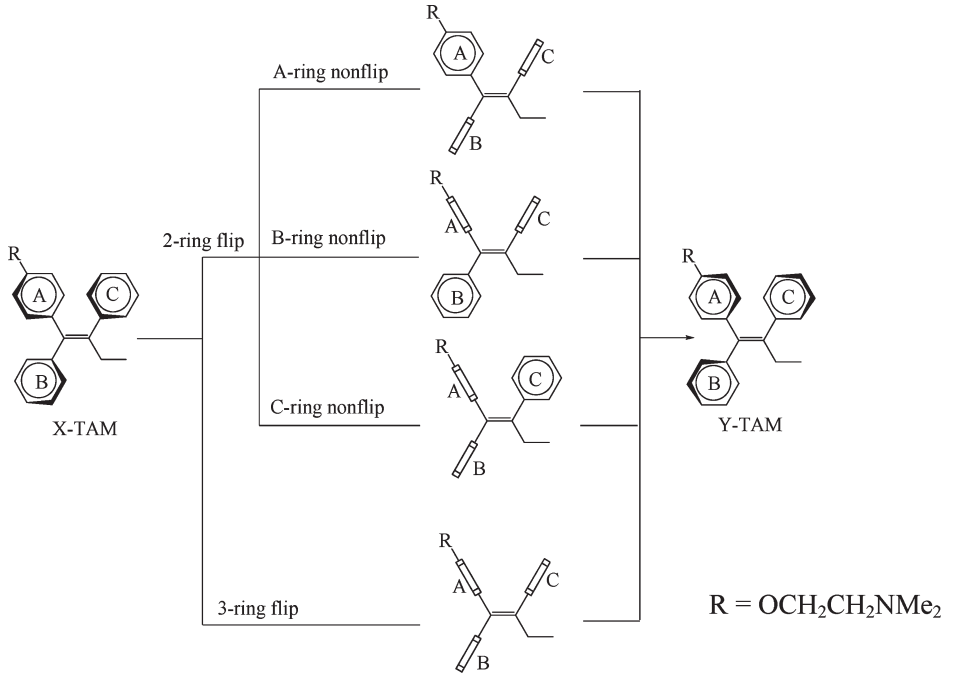

Figure 3. Idealized structures of the competing enantiomerization mechanisms. The transition states are shown in the middle. Rings in the perpendicular plane are denoted as ▭.

Table 2. Energy Barriers and Torsional Angles of the Enantiomerization Transition States for TAM Calculated at the B3LYP/6-31+G(d,p) Level

	energy barrier (kcal/mol)	torsional angle at TS (degrees)
$TS_{A\text{-ring nonflip}}$	3.78	$\alpha = -7.4$
$TS_{B\text{-ring nonflip}}$	8.29	$\beta = -5.9$
$TS_{C\text{-ring nonflip}}$	8.19	$\gamma = 0.9$
$TS_{Three\text{-ring flip}}$	3.20	

The three-ring flip probed by the different rotation-initiating rings, show identical transition states, which corroborates a correlated rotation of the aryl rings, i.e., helical inversion in this case takes place through a simultaneous motion of the three "blades".

The rotational transition states for the competing enantiomerization routes were optimized in vacuo, with the computed energy barriers listed in Table 2. The three-ring flip is found to have the lowest activation energy (3.2 kcal/mol), i.e., it is the threshold enantiomerization mechanism. The two-ring flips have higher barriers: 3.8−8.3 kcal/mol. Of these, the middle-ring (A-ring) nonflip exhibits much lower energy barriers than those of the other two and only slightly higher than that of the three-ring flip. Therefore, the middle-ring nonflip is also a possible route for the helical reversion, besides the threshold mechanism.

As mentioned in the Methodology section, test calculations were carried out using different DFT functionals with the 6-31+G(d,p) basis set. All functionals tested gave relatively low rotational barriers (3.6−4.9 kcal/mol) for the A-ring nonflip (Table S1 of the Supporting Information). More test calculations were performed on the rotational barriers of the biphenyl systems, which is a highly conjugated system comparable to TAM. A range of basis sets were used with the B3LYP and BLYP methods. Further improvement was obtained when the more extended 6-311++G(2d,2p) basis set was used. The results are in reasonable agreement with experimental data (Figure S2 and Table S1 of the Supporting Information).

Table 3. ZPE Corrected Rotational Barriers of the Enantiomerization Processes Calculated at the B3LYP and BLYP Levels with the 6-311++G(2d,2p) Basis Set[a]

		B3LYP		BLYP	
		$\Delta E_{(ZPE)}$	$\Delta\Delta E_{(ZPE)}$	$\Delta E_{(ZPE)}$	$\Delta\Delta E_{(ZPE)}$
TAM	X-TAM	−1138.390069	0	−1137.871198	0
	$TS_{A\text{-ring nonflip}}$	−1138.384071	3.76	−1137.865360	3.66
	$TS_{B\text{-ring nonflip}}$	−1138.377064	8.16	−1137.858718	7.83
	$TS_{C\text{-ring nonflip}}$	−1138.376958	8.23	−1137.858586	7.91
	$TS_{Three\text{-ring flip}}$	−1138.386210	2.42	−1137.867402	2.38
OHT	X−OHT	−1213.636144	0	−1213.11305	0
	$TS_{A\text{-ring nonflip}}$	−1213.629789	3.99	−1213.10685	3.89
	$TS_{B\text{-ring nonflip}}$	−1213.623789	7.75	−1213.101186	7.44
	$TS_{C\text{-ring nonflip}}$	−1213.622525	8.55	−1213.099882	8.26
	$TS_{Three\text{-ring flip}}$	−1213.631717	2.78	−1213.108728	2.71

[a] Absolute energies are in a.u., and relative energies are in kcal/mol.

To this end, B3LYP and BLYP methods with the 6-311++G(2d,2p) basis set were used to further calculate the rotational barriers of TAM and the more potent anti-estrogen 4-hydroxy metabolite. Again, lower energy barriers were obtained for the threshold mechanism when the more extended 6-311++G(2d,2p) basis set was used, compared to 6-31+G(d,p) (Table 3). The addition of the hydroxyl group at the B-ring *para*-position only slightly modifies the barriers of enantiomerization, as the substitution is a small group and lies along the rotational axis. The *para*-substitution does not alter the threshold rotational route, the three-ring flip, although the lowest activation barriers are increased by ∼0.3 kcal/mol. For the two-ring flips, the hydroxyl

dx.doi.org/10.1021/ci100401t |*J. Chem. Inf. Model.* 2011, 51, 306–314

Table 4. Enantiomerization Free Energies of TAM and OHT in Gas Phase and in Aqueous Solution at 298 K, Calculated at the B3LYP and BLYP Levels with the 6-311++G(2d,2p) Basis Set[a]

		ΔG_{gas}^{298}	$\Delta\Delta G_{gas}^{298}$	ΔG_{aq}^{298}	$\Delta\Delta G_{aq}^{298}$
		TAM			
B3LYP	X-TAM	−1138.451268	0	−1138.546663	0
	$TS_{A\text{-ring nonflip}}$	−1138.443265	5.02	−1138.536915	6.12
	$TS_{B\text{-ring nonflip}}$	−1138.437699	8.51	−1138.531152	9.73
	$TS_{C\text{-ring nonflip}}$	−1138.436200	9.46	−1138.532617	8.81
	$TS_{Three\text{-ring flip}}$	−1138.447269	2.51	−1138.541852	3.02
BLYP	X-TAM	−1137.933528	0	−1138.026927	0
	$TS_{A\text{-ring nonflip}}$	−1137.925389	5.11	−1138.017351	6.01
	$TS_{B\text{-ring nonflip}}$	−1137.919486	8.81	−1138.011767	9.51
	$TS_{C\text{-ring nonflip}}$	−1137.918868	9.20	−1138.014482	7.81
	$TS_{Three\text{-ring flip}}$	−1137.929204	2.71	−1138.02288	2.54
		OHT			
B3LYP	X−OHT	−1213.698635	0	−1213.801621	0
	$TS_{A\text{-ring nonflip}}$	−1213.691089	4.74	−1213.793122	5.33
	$TS_{B\text{-ring nonflip}}$	−1213.684152	9.09	−1213.786731	9.34
	$TS_{C\text{-ring nonflip}}$	−1213.683738	9.35	−1213.785962	9.83
	$TS_{Three\text{-ring flip}}$	−1213.693212	3.40	−1213.795477	3.86
BLYP	X−OHT	−1213.176659	0	−1213.277634	0
	$TS_{A\text{-ring nonflip}}$	−1213.169456	4.52	−1213.268342	5.83
	$TS_{B\text{-ring nonflip}}$	−1213.162487	8.89	−1213.262283	9.63
	$TS_{C\text{-ring nonflip}}$	−1213.162523	8.87	−1213.26128	10.26
	$TS_{Three\text{-ring flip}}$	−1213.171214	3.42	−1213.273524	2.58

[a] Absolute energies are in a.u., and relative energies are in kcal/mol.

group reduces the energy barriers by ∼0.4 kcal/mol for the B-ring nonflip but increases the energy barriers by ∼0.3 kcal/mol for the A-ring nonflip and C-ring nonflip. That is, the hydroxyl group slightly reduces the energy barriers when the substituted ring is the one rotating through the double-bond plane and slightly increases the energy barriers of the other two nonflip processes.

Exploring the enantiomerization processes in aqueous solution provides insight into the motion of the anticancer drug TAM and its metabolites under physiological conditions. To this end, PCM calculations were performed to model bulk solvent effects. The results, displayed in Table 4, show that the aqueous environment does not influence the threshold enantiomerization route, i.e., the three-ring flip still has the lowest activation energy. The heights of the rotational barriers are slightly modified by the polar medium, amounting to approximately 3 kcal/mol and 4 kcal/mol for the threshold mechanisms of TAM and OHT, respectively. There is slight difference between ZPE corrected barriers and Gibbs free energy barriers due to the entropic contributions; similar effects are also found in previous studies.[31−33] The activation barriers are much lower than for systems having more crowded vinyl propellers (15−20 kcal/mol), which, as opposed to the current systems, are detectable by NMR experiments. The current barriers, 3−4 kcal/mol, are easily overcome by thermal motion at physiologically relevant temperatures, which indicate fast interconversion between the enantiomers in vivo.

Demethylation of the bulky tails giving the two common derivatives N-desmethyl-TAM and 4-OH-N-desmethyl-TAM (edoxifen) has no obvious effect on the total energy barriers (Table S4 of the Supporting Information). Thus, the enantiomerization processes of N-desmethyl-TAM and endoxifen are similar to those found for TAM and OHT. TAM and its main metabolites, hence, all exist with equal populations of their two enantiomers under physiological conditions, although the precise mode of anti-estrogenic action of the enantiomeric pairs is unclear.

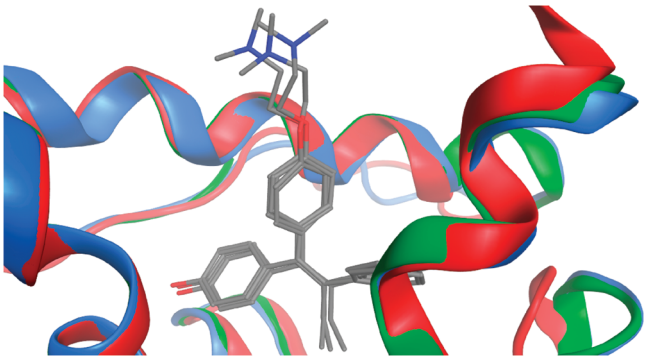

Figure 4. Superimposed crystallographic structures of OHT in complex with ERα LBD, 3ERT (red),[4] 2JF9.A (blue),[34] and 2BJ4.A (green).[35].

Table 5. Torsional Angles of X-ray Data of OHT/GW5638 Cocrystallined with ERα LBD, Compared with Crystalline TAM

	torsional angle (degrees)				
	α	β	γ	δ	conformer
ligand OHT (3ERT)	47	47	51	−115	X
ligand OHT (2JF9.A)	61	57	64	−133	X
ligand OHT (2BJ4.A)	56	55	58	−127	X
ligand GW5638 (1R5K)	31	53	47	−127	X
TAM	−48	64	55	114	Y

Not surprisingly, the difference in these enantiomers has essentially been completely neglected in the biological studies. The enantiomerization barriers (3−4 kcal/mol) of the drug TAM and its derivatives are not high enough to allow for the isolation of either of the enantiomeric conformers. Therefore, it is not possible to detect the pharmacological profiles of the two chiral forms experimentally. Further computational studies were therefore carried out herein to model the binding of the atropisomeric derivatives to ERα.

3.2. Enantioselectivity of ERα. Three cocrystallized structures of OHT and ERα have been solved and deposited in the PDB by different research groups. Superposition of these X-ray structures is shown in Figure 4. The backbones of the three structures overlap well, with an rmsd value of 0.75 Å. The blades of the vinyl propellers are twisted in the same sense and match in helicity; this is also the case for another triarylvinyl compound, GW5638, in complex with ERα (Figure S2 and Scheme S1 of the Supporting Information). The torsional angles of the vinyl propellers of OHT and GW5638 cocrystallized with ERα LBD were measured, showing that only the "clockwise" propellers (conformer X) are found in the ERα ligand binding pocket (Table 5). Crystalline TAM, on the other hand, exits in the "counterclockwise" propeller (conformer Y). That is, the crystalline state of TAM favors the Y conformer, while the ERα ligand binding pocket favors the X conformer. Further investigations

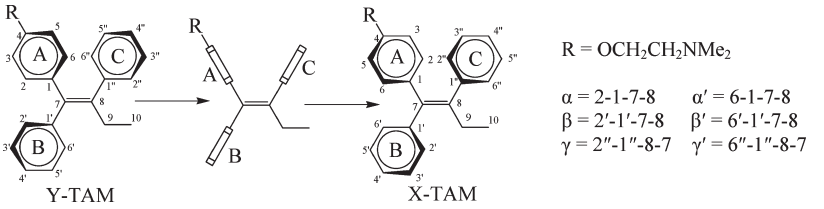

Figure 5. The overall C_1 symmetry of TAM through the three-ring flip.

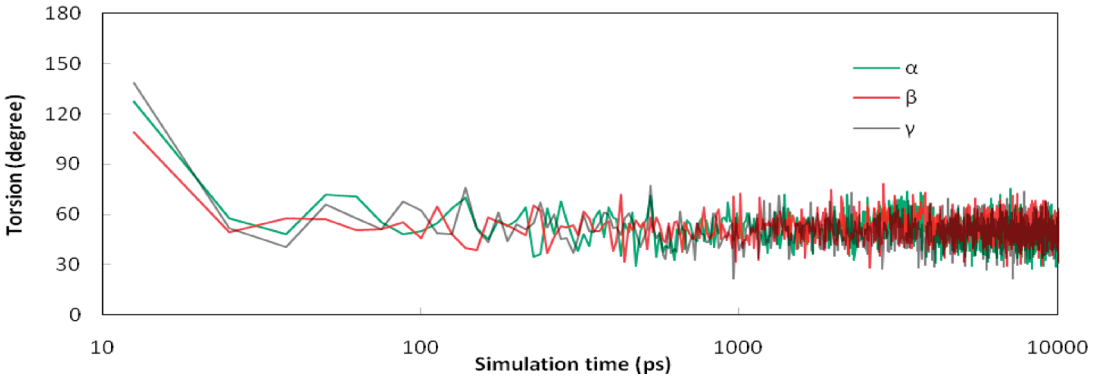

Figure 6. Dynamical motion of torsional angles α, β, and γ of TAM in the ERα ligand binding pocket during 10 ns MD.

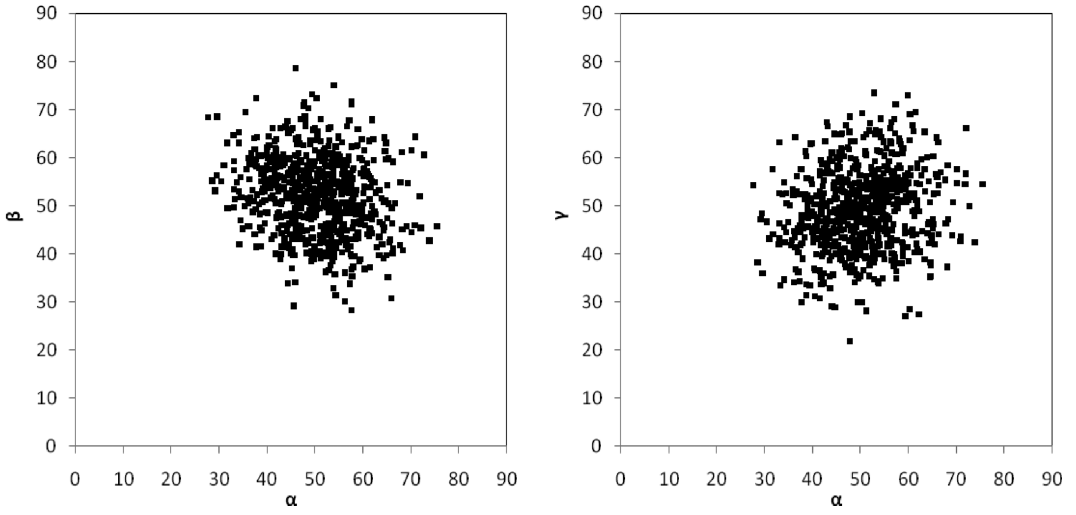

Figure 7. Distribution plots of torsional angles of TAM in the ERα ligand binding pocket during MD time range of 1−10 ns (after equilibrium).

were therefore performed using MD simulations by introducing the Y conformer to the ERα pocket.

Three independent 10 ns molecular dynamics simulations were conducted for Y-TAM−ERα LBD, where the Y-form of TAM was originally placed in the binding pocket and then allowed to move freely (no constrains) during the simulation. Although each aryl ring of TAM has the local C_2 axis, the overall C_1 symmetry needs to be considered to investigate the atomic motions as shown in Figure 5. The torsional angles of Y-TAM in the simulation starting point were set as −47°, −47°, and −51° for α′, β', and γ', respectively, i.e., 142°, 130°, and 140° for α, β, and γ, respectively. The trajectories of the torsional angles α, β, and γ in the ERα binding site were monitored as shown for one of the simulations in Figure 6. For all systems, Y-to-X conversion was observed to occur through the three-ring flip mechanism at the beginning of the simulation, whereafter TAM maintained in the ERα-favored X conformer throughout the remaining simulation time. The systems equilibrated within 1 ns, giving a distribution plot of torsional angles in ERα pocket after equilibrium (1−10 ns) as shown in Figure 7.

To examine the binding energy of Y-TAM and X-TAM in the ERα LBD, the torsional angles α, β, and γ were fixed as 47°, 47°, and 51° for X-TAM−ERα LBD, and 142°, 130°, and 140° for Y-TAM−ERα LBD. Separate simulations were conducted for 1 ns for the two fixed structures to allow these to find their optimal interaction with the binding pocket. The binding energies subsequently obtained were 154 kcal/mol and 94 kcal/mol for X-TAM and Y-TAM, respectively, indicating a 60 kcal/mol preference in binding of the X conformer.

Three independent 10 ns simulations without constrains were also conducted with Y-OHT−ERα LBD as the starting point. The dynamic behavior (Figure S3 of the Supporting Information)

dx.doi.org/10.1021/ci100401t |J. Chem. Inf. Model. 2011, 51, 306–314

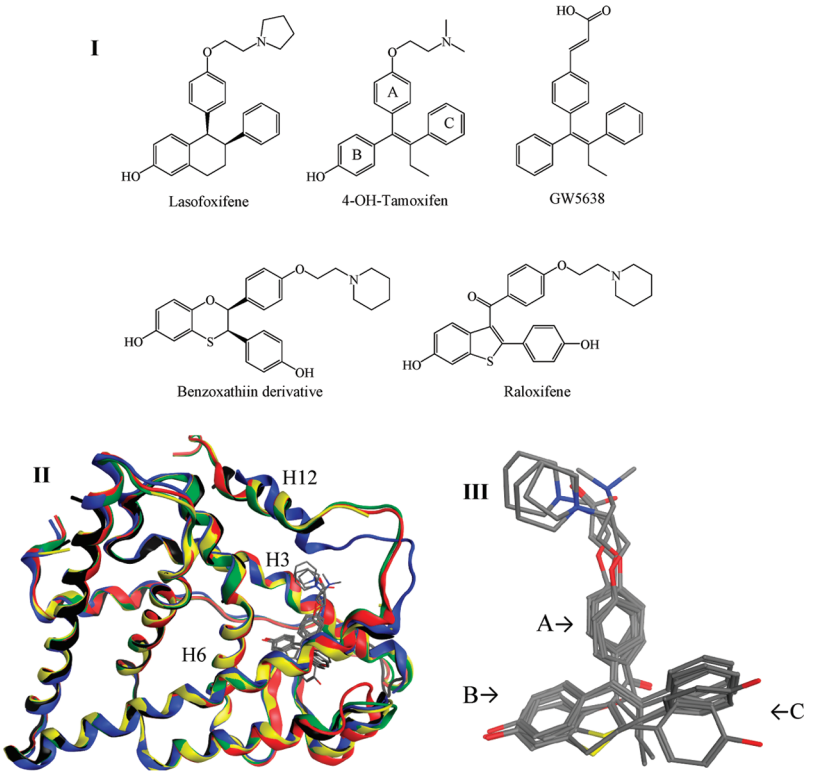

Figure 8. I. SERMs used in the superposition comparison. II. Superposed backbones of ERα LBD crystal structures with different SERMs: 1ERR-raloxifene (black),[37] 1R5K-GW5638 (blue),[38] 2OUZ-lasofoxifene (green),[39] 3ERT-4OH-TAM (red),[4] and 1SJ0-benzoxathiin derivative (yellow).[40] III. The ligands in the superposed backbones.

was found to be highly similar to that of TAM. Y-to-X conversion was observed in all repeating simulations, whereas the X-to-Y conversion was not observed. These observations indicate that the Y enantiomers are discriminated by ERα, which is consistent with the experimental work of TAM analogues showing that these torsional angles correlate to the relative binding affinity to ER.[19] It confirms the importance of the torsional angles for the ligands to fit properly into the pocket. This conclusion is also supported by experimental work of 1,1-diarylethylene analogues, showing that unfavored torsional angles dramatically reduced the binding affinity to ERα for similar ligands[36] (Table S4 of the Supporting Information).

More structural studies were performed to gain further understanding of the three-dimensional nature of the ERα binding pocket. Crystallographic structures of wild type ERα LBD in complex with five different SERMs were chosen (Figure 8). Superposition of the crystallographic structures of the five different SERM−ERα LBD complexes display highly conserved structures, despite the different structures of the ligands. The superposed backbones of the ERα LBD are essentially identical in most parts of the receptor. The calculated rmsd value of the C-α atoms is only 1.2 Å. The superposed ligands in the binding site show an identical binding mode for all the five SERMs. The phenolic hydroxyl groups of the B-rings are situated in the same region, and the entire B-rings wedge into the receptor in the same orientation. The ligands are then pinched by two rigid helixes, H6 and H3, thereby determining the favorable torsional angles of the aryl rings to binding ERα. This part of the ERα pocket is the most rigid region. All the A-rings and B-rings of the five ligands bind to the pocket in very similar orientations despite their diverse structures. Orientational changes of the C-rings are much more tolerable for the receptor. There is furthermore considerable room in this part of the pocket to accommodate variations and substituents on the C-ring moiety.

4. CONCLUSIONS

The DFT studies confirm that the helicity reversal in TAM propellers (conformer X and Y) proceed by a correlated rotation of the rings. The three-ring flip was revealed as the rotational threshold mechanism for TAM derivatives, consistent with the experimental studies of more crowded vinyl propellers. TAM and its metabolites studied herein have the same rotational threshold mechanism in gas phase and solvent, with similar low rotational barriers (3−4 kcal/mol). The barriers are not sufficiently high to enable separation of their torsional enantiomers. Because of the rapid interconversion between the two torsional enantiomers to racemates in the physiological environment, the pharmacological profiles of the two chiral forms are not detectable experimentally for the anticancer drug TAM and its metabolites.

For this reason, structure studies have been performed on the drug target ERα. We have compared the cocrystallized structures of diverse ligands in complex with the ERα LBD to study the plasticity of the receptor. The LBD is rigid in structure except for the flexible helix H12 located at the C-terminal. The torsional angles of the aryl rings of TAM derivatives are restrained in the binding pocket by the rigid helixes H3 and H6. As a result, only the "clockwise" propeller structures (conformer X) of different TAM derivatives bind to ERα. The aryl ring orientations of the ligands greatly influence

their capacity to bind to ERα, and MD simulations revealed a very rapid conversion from the inactive Y-form to the X-form. In addition, there is a significant difference in binding energy of the two conformers to the ERα LBD. The modeling results are in good agreement with experimental data showing that unfavored torsional angles dramatically reduces the binding affinity to ERα for similar ligands. ERα shows enantioselectivity of ligands with chiral propeller conformations, which indicates distinctly different pharmacological profiles of the two enantiomers, i.e., conformer X is more potent than conformer Y. Such chiral selectivity of ERα should be considered when searching for new lead compounds.

The important biotransformation pathways of TAM in vivo are 4-hydroxylation and N-desmethylation of the bulky tail. All these metabolites display similar low rotational energy barriers, such that TAM and its metabolites easily convert to the favored conformer X when binding to ERα. Hence, the enatiomerization of TAM derivatives are correlated with their fitting into the 3-D structure of the ERα ligand binding pocket and their capability to function as estrogen agonists or antagonists.

■ ASSOCIATED CONTENT

Supporting Information. Results of test and benchmark calculations and additional information discussed herein. This material is available free of charge via the Internet at http://pubs.acs.org.

■ AUTHOR INFORMATION

Corresponding Author
*E-mail: leif.eriksson@nuigalway.ie.

■ ACKNOWLEDGMENT

Financial support from the Swedish Science Research Council, Faculty of Science and Technology at Örebro University, and National University of Ireland, Galway, is gratefully acknowledged.

■ REFERENCES

(1) Ingle, J. N.; Ahmann, D. L.; Green, S. J.; Edmonson, J. H.; Bisel, H. F.; Kvols, L. K.; Nichols, W. C.; Creagan, E. T.; Hahn, R. G.; Rubin, J.; Frytak, S. Randomized clinical trial of diethylstilbestrol versus tamoxifen in postmenopausal women with advanced breast cancer. *N. Engl. J. Med.* **1981**, *304*, 16–21.

(2) Furr, B. J.; Jordan, V. C. The pharmacology and clinical uses of tamoxifen. *Pharmacol. Ther.* **1984**, *25*, 127–205.

(3) Clarke, M.; Collins, R.; Davies, C.; Godwin, J.; Gray, R.; Peto, R.; Grp, E. B. C. T. C. Tamoxifen for early breast cancer: An overview of the randomised trials. *Lancet* **1998**, *351*, 1451–1467.

(4) Shiau, A. K.; Barstad, D.; Loria, P. M.; Cheng, L.; Kushner, P. J.; Agard, D. A.; Greene, G. L. The structural basis of estrogen receptor/coactivator recognition and the antagonism of this interaction by tamoxifen. *Cell* **1998**, *95*, 927–37.

(5) Jin, Y.; Desta, Z.; Stearns, V.; Ward, B.; Ho, H.; Lee, K. H.; Skaar, T.; Storniolo, A. M.; Li, L.; Araba, A.; Blanchard, R.; Nguyen, A.; Ullmer, L.; Hayden, J.; Lemler, S.; Weinshilboum, R. M.; Rae, J. M.; Hayes, D. F.; Flockhart, D. A. CYP2D6 genotype, antidepressant use, and tamoxifen metabolism during adjuvant breast cancer treatment. *J. Natl. Cancer Inst.* **2005**, *97*, 30–39.

(6) Desta, Z.; Ward, B. A.; Soukhova, N. V.; Flockhart, D. A. Comprehensive evaluation of tamoxifen sequential biotransformation by the human cytochrome P450 system in vitro: Prominent roles for CYP3A and CYP2D6. *J. Pharmacol. Exp. Ther.* **2004**, *310*, 1062–1075.

(7) Fabian, C.; Tilzer, L.; Sternson, L. Comparative binding affinities of tamoxifen, 4-hydroxytamoxifen, and desmethyltamoxifen for estrogen receptors isolated from human breast carcinoma: Correlation with blood levels in patients with metastatic breast cancer. *Biopharm. Drug Dispos.* **1981**, *2*, 381–390.

(8) Johnson, M. D.; Zuo, H.; Lee, K. H.; Trebley, J. P.; Rae, J. M.; Weatherman, R. V.; Desta, Z.; Flockhart, D. A.; Skaar, T. C. Pharmacological characterization of 4-hydroxy-N-desmethyl tamoxifen: A novel active metabolite of tamoxifen. *Breast Cancer Res. Treat.* **2004**, *85*, 151–159.

(9) Precigoux, G.; Courseille, C.; Geoffre, S.; Hospital, M. [p-(Dimethylamino-2-ethoxy)phenyl]-1-trans-diphenyl-1,2-butene-1-(tamoxifen)(ICI-46474). *Acta Crystallogr., Sect. B: Struct. Sci.* **1979**, *35*, 3070–3072.

(10) Biali, S. E.; Rappoport, Z. Stable simple enols. 3. Static and dynamic NMR behavior of crowded triarylethenols and related compounds: Three-ring flip as the threshold mechanism for enantiomerization of crowded triarylvinyl propellers. *J. Am. Chem. Soc.* **1984**, *106*, 477–496.

(11) Kaftory, M.; Biali, S. E.; Rappoport, Z. Stable simple enols. 9. Solid-state structures and conformations of several simple enols and their keto tautomers. *J. Am. Chem. Soc.* **1985**, *107*, 1701–1709.

(12) Rappoport, Z.; Biali, S. E. Threshold rotational mechanisms and enantiomerization barriers of polyarylvinyl propellers. *Acc. Chem. Res.* **1997**, *30*, 307–314.

(13) Kuramochi, H. Conformational studies and electronic structures of tamoxifen and toremifene and their allylic carbocations proposed as reactive intermediates leading to DNA adduct formation. *J. Med. Chem.* **1996**, *39*, 2877–2886.

(14) Schmittel, M.; Keller, M.; Burghart, A.; Rappoport, Z.; Langels, A. Electronic effects in polyarylvinyl propellers. Solid state structures and dynamic behaviour in solution of several crowded enol derivatives. *J. Chem. Soc., Perkin Trans. 2* **1998**, 869–875.

(15) Rochlin, E.; Rappoport, Z.; Kastner, F.; Pustet, N.; Mannschreck, A. Four enantiomerization routes of 1,2,2-trimesitylvinyl acetate. Enantioselective liquid chromatography of (*E*)- and (*Z*)-2-m-methoxymesityl-1,2-dimesitylvinyl acetates. *J. Org. Chem.* **1999**, *64*, 8840–8845.

(16) Biali, S. E.; Kaftory, M.; Rappoport, Z. Restricted rotation and torsional isomerism in tamoxifen derivatives. *J. Org. Chem.* **1989**, *54*, 4959–4962.

(17) Rochlin, E.; Rappoport, Z. Mapping the enantiomerization routes of triarylvinyl propellers: Barriers for the three-ring flip and the three different two-ring flips of m-methoxy-substituted trimesitylvinyl isopropyl ethers. *J. Org. Chem.* **1994**, *59*, 3857–3870.

(18) Biali, S. E.; Rappoport, Z. A two-ring flip as the threshold enantiomerization route for a triarylvinyl propeller. 1D and 2D NMR and static and dynamic stereochemistry of trimesitylethylene. *J. Org. Chem.* **1986**, *51*, 2245–2250.

(19) McCague, R.; Kuroda, R.; Leclercq, G.; Stoessel, S. Synthesis and estrogen receptor binding of 6,7-dihydro-8-phenyl-9-[4-[2-(dimethylamino)ethoxy] phenyl]-5H-benzocycloheptene, a nonisomerizable analogue of tamoxifen. X-ray crystallographic studies. *J. Med. Chem.* **1986**, *29*, 2053–9.

(20) Becke, A. D. Density-functional thermochemistry. III. The role of exact exchange. *J. Chem. Phys.* **1993**, *98*, 5648–5652.

(21) Lee, C. T.; Yang, W. T.; Parr, R. G. Development of the Colle−Salvetti correlation-energy formula into a functional of the electron density. *Phys. Rev. B* **1988**, *37*, 785–789.

(22) Stephens, P. J.; Devlin, F. J.; Chabalowski, C. F.; Frisch, M. J. Ab initio calculation of vibrational absorption and circular dichroism spectra using density functional force fields. *J. Phys. Chem.* **1994**, *98*, 11623–11627.

(23) Marenich, A. V.; Cramer, C. J.; Truhlar, D. G. Universal solvation model based on solute electron density and on a continuum model of the solvent defined by the bulk dielectric constant and atomic surface tensions. *J. Phys. Chem. B* **2009**, *113*, 6378–6396.

(24) Frisch, M. J.; Trucks, G. W.; Schlegel, H. B.; Scuseria, G. E.; Robb, M. A.; Cheeseman, J. R.; Scalmani, G.; Barone, V.; Mennucci, B.; Petersson, G. A.; Nakatsuji, H.; Caricato, M.; Li, X.; Hratchian, H. P.; Izmaylov, A. F.; Bloino, J.; Zheng, G.; Sonnenberg, J. L.; Hada, M.;

Ehara, M.; Toyota, K.; Fukuda, R.; Hasegawa, J.; Ishida, M.; Nakajima, T.; Honda, Y.; Kitao, O.; Nakai, H.; Vreven, T.; Montgomery, J. A.; Jr.; Peralta, J. E.; Ogliaro, F.; Bearpark, M.; Heyd, J. J.; Brothers, E.; Kudin, K. N.; Staroverov, V. N.; Kobayashi, R.; Normand, J.; Raghavachari, K.; Rendell, A.; Burant, J. C.; Iyengar, S. S.; Tomasi, J.; Cossi, M.; Rega, N.; Millam, J. M.; Klene, M.; Knox, J. E.; Cross, J. B.; Bakken, V.; Adamo, C.; Jaramillo, J.; Gomperts, R.; Stratmann, R. E.; Yazyev, O.; Austin, A. J.; Cammi, R.; Pomelli, C.; Ochterski, J. W.; Martin, R. L.; Morokuma, K.; Zakrzewski, V. G.; Voth, G. A.; Salvador, P.; Dannenberg, J. J.; Dapprich, S.; Daniels, A. D.; Farkas, O.; Foresman, J. B.; Ortiz, J. V.; Cioslowski, J.; Fox, D. J. Gaussian 09, Revision A.02; Gaussian, Inc.: Wallingford CT, 2009.

(25) Johansson, M. P.; Olsen, J. Torsional barriers and equilibrium angle of biphenyl: Reconciling theory with experiment. *J. Chem. Theory Comput.* **2008**, *4*, 1460–1471.

(26) *Molecular Operating Enviroment (MOE)*, version 2009.10. Chemcal Computing Group: Montreal, Canada, 2009.

(27) Krieger, E.; Darden, T.; Nabuurs, S. B.; Finkelstein, A.; Vriend, G. Making optimal use of empirical energy functions: Force field parameterization in crystal space. *Proteins: Struct., Funct., Bioinf.* **2004**, *57*, 678–683.

(28) Duan, Y.; Wu, C.; Chowdhury, S.; Lee, M. C.; Xiong, G.; Zhang, W.; Yang, R.; Cieplak, P.; Luo, R.; Lee, T.; Caldwell, J.; Wang, J.; Kollman, P. A point-charge force field for molecular mechanics simulations of proteins based on condensed-phase quantum mechanical calculations. *J. Comput. Chem.* **2003**, *24*, 1999–2012.

(29) Jakalian, A.; Jack, D. B.; Bayly, C. I. Fast, efficient generation of high-quality atomic charges. AM1-BCC model: II. Parameterization and validation. *J. Comput. Chem.* **2002**, *23*, 1623–1641.

(30) Huang, M. J. Ab initio studies of tamoxifen and related compounds. *Int. J. Quantum Chem.* **2004**, *96*, 374–379.

(31) Bren, U.; Zupan, M.; Guengerich, F. P.; Mavri, J. Chemical reactivity as a tool to study carcinogenicity: Reaction between chloroethylene oxide and guanine. *J. Org. Chem.* **2006**, *71*, 4078–4084.

(32) Bren, U.; Guengerich, F. P.; Mavri, J. Guanine alkylation by the potent carcinogen aflatoxin B-1: Quantum chemical calculations. *Chem. Res. Toxicol.* **2007**, *20*, 1134–1140.

(33) Galesa, K.; Bren, U.; Kranjc, A.; Mavri, J. Cinogenicity of acrylamide: A computational study. *J. Agric. Food Chem.* **2008**, *56*, 8720–8727.

(34) Heldring, N.; Pawson, T.; McDonnell, D.; Treuter, E.; Gustafsson, J. A.; Pike, A. C. Structural insights into corepressor recognition by antagonist-bound estrogen receptors. *J. Biol. Chem.* **2007**, *282*, 10449–55.

(35) Kong, E. H.; Heldring, N.; Gustafsson, J. A.; Treuter, E.; Hubbard, R. E.; Pike, A. C. Delineation of a unique protein−protein interaction site on the surface of the estrogen receptor. *Proc. Natl. Acad. Sci. U. S. A.* **2005**, *102*, 3593–8.

(36) Muthyala, R. S.; Sheng, S.; Carlson, K. E.; Katzenellenbogen, B. S.; Katzenellenbogen, J. A. Bridged bicyclic cores containing a 1,1-diarylethylene motif are high-affinity subtype-selective ligands for the estrogen receptor. *J. Med. Chem.* **2003**, *46*, 1589–602.

(37) Brzozowski, A. M.; Pike, A. C.; Dauter, Z.; Hubbard, R. E.; Bonn, T.; Engstrom, O.; Ohman, L.; Greene, G. L.; Gustafsson, J. A.; Carlquist, M. Molecular basis of agonism and antagonism in the oestrogen receptor. *Nature* **1997**, *389*, 753–8.

(38) Wu, Y. L.; Yang, X.; Ren, Z.; McDonnell, D. P.; Norris, J. D.; Willson, T. M.; Greene, G. L. Structural basis for an unexpected mode of SERM-mediated ER antagonism. *Mol. Cell* **2005**, *18*, 413–24.

(39) Vajdos, F. F.; Hoth, L. R.; Geoghegan, K. F.; Simons, S. P.; LeMotte, P. K.; Danley, D. E.; Ammirati, M. J.; Pandit, J. The 2.0 A crystal structure of the ERalpha ligand-binding domain complexed with lasofoxifene. *Protein Sci.* **2007**, *16*, 897–905.

(40) Kim, S.; Wu, J. Y.; Birzin, E. T.; Frisch, K.; Chan, W.; Pai, L. Y.; Yang, Y. T.; Mosley, R. T.; Fitzgerald, P. M.; Sharma, N.; Dahllund, J.; Thorsell, A. G.; DiNinno, F.; Rohrer, S. P.; Schaeffer, J. M.; Hammond, M. L. Estrogen receptor ligands. II. Discovery of benzoxathiins as potent, selective estrogen receptor alpha modulators. *J. Med. Chem.* **2004**, *47*, 2171–5.